Part I

Si and Ge Dots

ULTRAFAST ELECTRON DYNAMICS IN Ge QUANTUM DOTS

A. STELLA*, P. TOGNINI*, S. DE SILVESTRI**, M. NISOLI**, S. STAGIRA**, P. CHEYSSAC***, R. KOFMAN***

*Istituto Nazionale per la Fisica della Materia - Dipartimento di Fisica "A. Volta", Università di Pavia, Via Bassi 6, I-27100 Pavia, Italy
** Istituto Nazionale per la Fisica della Materia - Dipartimento di Fisica Politecnico di Milano, Centro di Elettronica Quantistica e Strumentazione Elettronica - CNR, Milano, Italy
***Laboratoire de Physique de la Matière Condensée, URA 190, Université de Nice-Sophia Antipolis, 06108 Nice Cedex, France

ABSTRACT

An analysis of the ultrafast response of Ge quantum dots, with average radii of 4 nm and 16 nm, is reported here. Pump and probe experiments allowed investigation *of* the wavelength region between 450 and 750 nm, characterized by the absorption peaks due to the E_1 and $E_1+\Delta_1$ interband transitions. Two different time regimes have been identified: a first one ($\tau \leq 1$ ps) associated with pump-induced conduction band filling in the Γ-L direction in the Brillouin zone; a second one (τ up to 100 ps) associated with band gap renormalization caused by the carrier interaction in the conduction band. Quantum confinement effects show up in terms of size-dependent blueshift of the $E_1+\Delta_1$ spectral feature.

INTRODUCTION

The expected or realized achievements in terms of linear and nonlinear optical behavior of newly developed materials constitute the basis for new applications, including full potential all-optical signal processing. It is well known for instance that glasses containing metal nanoparticles exhibit interesting properties in this respect, due to local field enhancement near the metal surface plasma resonance [1]. Glasses containing semiconducting nanocrystals are less investigated; nevertheless they present interesting optical features, such as relevant third order nonlinearities [2]. III-V and II-VI quantum dots have been the object of the main experimental and theoretical work [2-4], and much less is known about the relaxation mechanisms in nanocrystals of indirect-gap materials. In the case of Ge, these studies have been until now restricted to a relatively limited number of works, essentially devoted to reach a more comprehensive picture of the electron dynamics in the bulk [5-7]. Time-resolved four-wave-mixing measurements on Ge nanocrystals were recently performed to study the intensity-dependent refractive index [8].

We report on the ultrafast relaxation process in two samples containing Ge nanoparticles with average radii of about 4 and 16 nm, in the spectral region correspondent to the E_1 and $E_1 + \Delta_1$ interband transitions. In bulk Ge these two spectral structures originate from transitions in a wide portion of the BZ in the Γ-L direction between nearly-parallel bands [9]. The constant distance between valence and conduction bands, which gives rise to the absorption peak, is the reason for its partly excitonic nature [9,10]: electrons and holes, being characterised by the same group velocity, produce stable pairs. This may cause the observed 1/R-like blueshift of the absorption peak when reducing the dot size (see Fig. 1).

Mat. Res. Soc. Symp. Proc. Vol. 571 © 2000 Materials Research Society

SAMPLES AND TECHNIQUES

The Ge nanocrystals investigated here are embedded in a film of alumina sitting on a sapphire substrate. The growth is based on an evaporation-condensation self-organized process in the liquid phase, and on the partially wetting character of Ge with respect to the matrix [10]. The balance of the surface tensions of Ge and alumina, allows obtaining nanoparticles with truncated spherical shape and a size dispersion $\sigma/R \leq 20\%$. The average radius of the investigated nanoparticles is respectively ~16 nm (Ge16) and ~4 nm (Ge4).

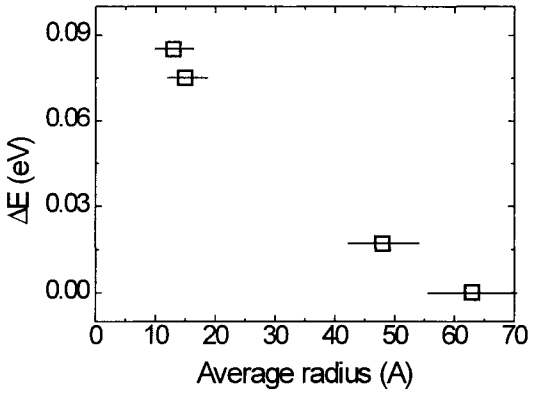

Figure 1. Blueshift of the $E_1+\Delta_1$ absorption peak as a function of the average radius of the nanoparticles (from ref. [10]).

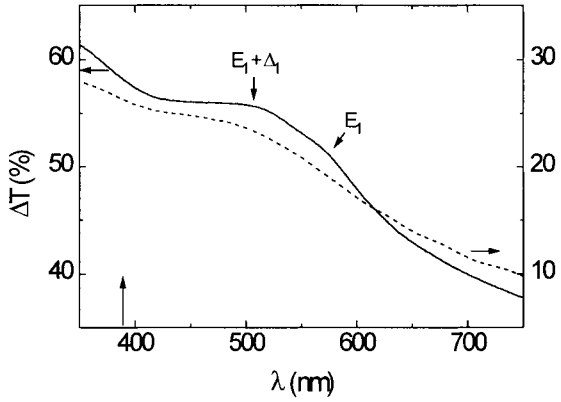

Figure 2. Difference between the transmittance of a reference sample without nanoparticles and the two investigated samples (Ge16: continuous line; Ge4: dashed line). The sapphire substrate and the alumina matrix does not present absorption structures in this spectral range.

Linear transmittance (Fig. 2) and reflectance measurements allowed us to obtain both the optical functions of the effective medium composed by nanoparticles + embedding matrix, and the position of the E_1 and $E_1+\Delta_1$ spectral structures.

Transient transmissivity measurements were performed by using a conventional pump-probe configuration. The laser system consists of a Ti:sapphire laser with chirped-pulse amplification, which provides pulses of 150-fs duration at 780 nm, with energy up to 750 μJ at 1-kHz repetition rate. The excitation pulses at 390 nm were generated by second harmonic conversion of the fundamental beam in a 1-mm-thick LiB_3O_5 crystal. The pump beam was focused to a spot of 80 μm diameter and the excitation fluence was ~0.6 mJ/cm^2 per pulse. Pump-probe experiments were carried out in the visible spectral range by using the white-light supercontinuum (as a probe) generated in a thin sapphire plate. Mirrors were used to collect the supercontinuum beam and to focus it on the samples in order to minimise frequency chirp effects. By carefully controlling the pulse energy and the position of the sapphire plate around the focus, it is possible to generate a remarkably stable continuum, of good optical quality and with smooth spectrum in the region from 450 to 700 nm. The white light shows a strong nonlinear chirp in proximity of the pump frequency, while over most of the visible the chirp is small and linear, with a group delay dispersion of approximately 100fs.

The number of quantum dots excited is related to the density of nanoparticles in each layer, which is around 10^{11} cm^{-2}. The measurements were carried out in the spectral range 450 - 750 nm.

EXPERIMENTAL RESULTS

The dominant absorption mechanism is given by single-photon interband transition near the Γ point of the Brillouin zone. The electrons initially created in the Γ valley scatter into the side valleys in about a hundred fs [6]. Once in the L valley, they thermalize with the lattice [11].

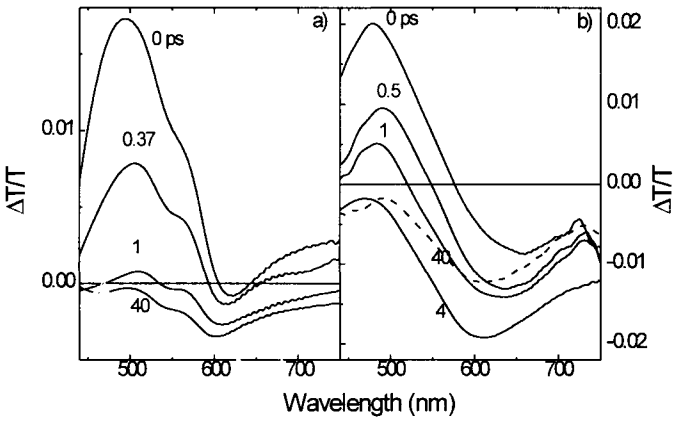

Figure 3: Differential transmission spectra of Ge16 (a) and Ge4 (b) for various pump-probe delays.

The ΔT/T spectra of the two Ge samples at room temperature are shown in Fig. 3 for different pump-probe delays τ_D. The bleaching (ΔT>0), which dominates the spectra at $\tau_D \leq 1$ps with a maximum at ~480 and ~490 nm in Ge4 and Ge16 respectively, corresponds to the position of the $E_1 + \Delta_1$ spectral structure of the Ge nanoparticles. The blueshift of this band in the smaller nanoparticles is in agreement with the values reported in Fig. 1. The bleaching band completely disappears in about 1 ps, and a broad photoinduced absorption (PA) band with a maximum at ~610 nm dominates the spectra of both samples at the longer delays.

We have associated the bleaching to the electron population, created by the pump pulse, which partially fills the conduction band along the Λ direction during its decay towards the L minimum [6]. This partial filling of the conduction states along the whole band in the Λ direction produces the spectral extension of the bleaching. Its decay time constant is associated with the transition of the electrons to the bottom of the band, so that a large part of the conduction states recover their initial condition.

The slower regime decays in some hundreds of ps, a time constant comparable to that which characterizes the band-to-band carrier recombination [12]. The driving mechanism which causes the shift of the spectral features due to interband transitions is given by population-induced band gap renormalization (BGR) [13]. It is well known that when a dense electron-hole plasma is formed in a semiconductor, electron-electron interactions lead to a narrowing of the gap. BGR, in this case, is caused by the electronic population of the conduction band in the Λ direction and is conserved after the relaxation towards the minimum, since it depends on the density of carriers rather than on their position in the band.

ANALYSIS

The above-described population-induced transmittance changes have been analyzed in terms of their influence on the dielectric function of the "effective medium" composed by Ge nanoparticles + matrix. This has allowed estimating the density of carriers created by the pump pulse and their initial temperature. The evaluation of the bleaching has been performed from the variation of the electron population in the conduction band (CB):

$$\frac{\Delta N}{N} \approx \frac{\Delta k}{k} = \frac{\Delta \alpha}{\alpha} \tag{1}$$

where N, k and α are respectively the carrier density, the extinction and the absorption coefficient.

With standard approximations related to the small thickness d of the effective layer, one has:

$$\frac{\Delta T}{T} \approx \frac{4\pi k}{\lambda} d \frac{\Delta N}{N} \tag{2}$$

The results of this calculation have been reported in fig. 4 (dashed line). The population induced BGR ΔE [15] has been calculated to be of the order of few meV. Its influence on the dielectric function can be evaluated using the expression $\Delta\varepsilon_{1,2} = \frac{\partial \varepsilon_{1,2}}{\partial E} \Delta E$ [16], where

$$\Delta E(N,T) = -\frac{4.64 N^{1/4}}{\left[N + (0.107T)^2\right]^{1/4}} \tag{3}$$

and carrier density N and temperature T are expressed in excitonic (or Rydberg) units [15].

The change in the dielectric function of Ge has been introduced in the effective medium formulation [17] to obtain the variation in the dielectric function of the composite medium, and consequently the $\Delta T/T$ reported in Fig. 4 (dotted line). The composition of the two effects is the continuous line in the same figure. Some hundred fs after the pump pulse, both bleaching and BGR are present, so that the $\Delta T/T$ curve is represented by the sum of the two effects (continuous line in Fig. 4). After about 1 ps, the $\Delta T/T$ curve is dominated by the BGR effect (dotted line in Fig. 4). The spectral behavior presents a good agreement with the experiment reported in Fig. 3.

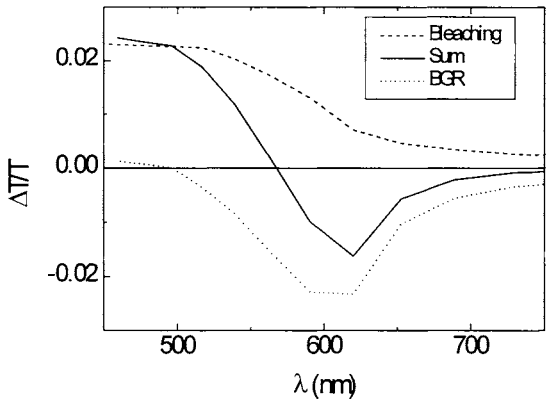

Figure 4: Effective medium (nanoparticles + matrix) differential transmittance: dotted line: contribution of the conduction band filling along the Λ direction (considering $\Delta N/N \sim 10^{-3}$; dashed line: contribution of the BGR; continuous line: sum of the two effects. Ge optical functions have been taken from ref. [14].

CONCLUSIONS

It has been demonstrated that in the spectral region analyzed, around the E_1 and $E_1+\Delta_1$ spectral structures, the optical response is characterised by a reduction of the differential transmittance around 500 nm immediately after the pump pulse, followed by an increased absorption at about 600 nm at longer delays. The origin of both phenomena is amenable to the carrier population effects in the conduction band.

We acknowledge financial support from Progetto Finalizzato Materiali e Dispositivi per l'Elettronica dello Stato Solido II (MADESS II).

REFERENCES

1. U. Kreibig and M. Vollmer, *Optical Properties of Metal Clusters* (Springer-Verlag, Berlin, 1995); A. Stella, M. Nisoli, S. De Silvestri, O. Svelto, G. Lanzani, P. Cheyssac, R. Kofman, Phys. Rev. B **53**, 15497 (1996).

2. U. Woggon, *Optical Properties of Semiconductor Quantum Dots* (Springer-Verlag, Berlin Heidelberg, 1997), and references therein.

3. D.M. Mittleman, R. W. Schoenlein, J. J. Shiang and V. L. Colvin, A. P. Alivisatos, and C. V. Shank, Phys. Rev. B **49**, 14435 (1994), and references therein.

4. U. Banin, G. Cerullo, A. A. Guzelian, C. J. Bardeen, A. P. Alivisatos, and C. V. Shank, Phys. Rev. B **55**, 7059 (1997).

5. X.Q. Zhou, H. M. van Driel, and G. Mak, Phys. Rev. B **50**, 5226 (1994); M. Woerner, W. Frey, M. T. Portella, C. Ludwig, T. Elsaesser, and W. Kaiser, Phys. Rev. B **49**, 17007 (1994).

6. S. Zollner, K.D. Myers, K.G. Jensen, J.M. Dolan, D.W. Bailey, C.J. Stanton, Sol. St. Comm. **104**, 51 (1997).

7. T. Rappen, U. Peter, M. Wegener, and W. Schäfer, Phys. Rev. B **48**, 4879 (1993); K. Tanaka, H. Ohtake, and T. Suemoto, Phys. Rev. Lett. **71**, 1935 (1993).

8. A. Dowd, R. G. Elliman, M. Samoc and B. Luther-Davies, Appl. Phys. Lett. **74**, 239 (1999).

9. M.L. Cohen and J.R. Chelikowsky, *Electronic Structure and Optical Properties of Semiconductors* (Springer-Verlag, Berlin, 1988).

10. P. Tognini, L.C. Andreani, M. Geddo, A. Stella, P. Cheyssac, R. Kofman and A.Migliori, Phys. Rev. B **53**, 6992 (1996); P. Tognini, L.C. Andreani, M. Geddo, A. Stella, P. Cheyssac and R. Kofman, Il Nuovo Cimento D **18**, 865 (1996).

11. A. Othonos, H.M. van Driel, J.F. Young and P.J. Kelly, Phys. Rev. B **43**, 6682 (1991).

12. J. Shah, *Ultrafast Spectroscopy of Semiconductors and Semiconductor Nanostructures* (Springer-Verlag, Berlin, 1996).

13. R. Haight, M. Baeumler, Phys. Rev. B **46**, 1543 (1992).

14. D.E. Aspnes and A.A. Studna, Phys. Rev. B **27**, 985 (1983).

15. R. Zimmermann, Phys. Stat. Sol. (b) **146**, 371 (1988).

16. H.R. Choo, X.F. Hu, M.C. Downer and V.P. Kesan, Appl. Phys. Lett. **63**, 1507 (1993).

17. L. Genzel and T.P. Martin, Surf. Sci. **34**, 33 (1973).

INTRABAND ABSORPTION IN Ge/Si SELF-ASSEMBLED QUANTUM DOTS

P. Boucaud*, V. Le Thanh*, S. Sauvage*, T. Brunhes*, F. Fortuna, D. Debarre*, D. Bouchier***

*** IEF, Université Paris XI, UMR CNRS 8622, Bât. 220, 91405 Orsay, FRANCE, phill@ief.u-psud.fr**
**** CSNSM, Université Paris XI, Bât. 108, 91405 Orsay, FRANCE**

ABSTRACT

Mid-infrared intraband absorption in Ge/Si self-assembled quantum dots is reported. The self-assembled quantum dots are grown by ultra-high-vacuum chemical vapor deposition. The intraband absorption is observed using a photoinduced absorption technique. The mid-infrared absorption, which is in-plane polarized, is maximum around 300 meV. The absorption is attributed to a quantum dot hole transition between bound and continuum states. The absorption cross section is deduced from the saturation of the photoinduced intraband absorption. An in-plane absorption cross section as large as 2×10^{-13} cm^2 is measured for one dot plane.

INTRODUCTION

The intraband transitions which occur between quantum confined states in the conduction or in the valence band of semiconductor quantum dots have become a new research subject in the last years. Intraband transitions have been mostly observed in III-V self-assembled quantum dots [1,2]. Most of the work reported to date was related to absorption although nonlinear optical measurements using intraband transitions has been recently reported [3]. The observation of mid-infrared absorption has opened the route to the development of new quantum dot infrared photodetectors. Mid-infrared photoconductivity using InAs self-assembled quantum dots has been first reported [4,5] shortly followed by the characterization of quantum dot devices [6,7].

Si-based self-assembled quantum dots are also attracting a lot of interest due to their compatibility with Si-based signal processing. Intraband transitions in these nanostructures have only been observed very recently [8,9]. These first observations are likely to lead to the realization of new Si-based quantum dot infrared photodetectors.

RESULTS

Growth and structural characterizations of Ge/Si self-assembled quantum dots

The self-assembled quantum dots were grown by ultra-high-vacuum chemical vapor deposition using silane and germane as gas precursors [10]. The samples, grown at 550° C, consist of 10 Ge layers separated by 22 nm thick Si barriers. Samples with different dot sizes were characterized. For infrared measurements, the samples were polished with 45° facets in a multipass waveguide geometry [2]. The self-assembled quantum dots are nominally undoped.

Mat. Res. Soc. Symp. Proc. Vol. 571 © 2000 Materials Research Society

A cross section electronic microscopy image of the 10 Ge layer sample is shown in figure 1. Due to the small thickness of the Si barrier, the quantum dots are vertically organized. As the number of layers increases, the quantum dot volume increases.

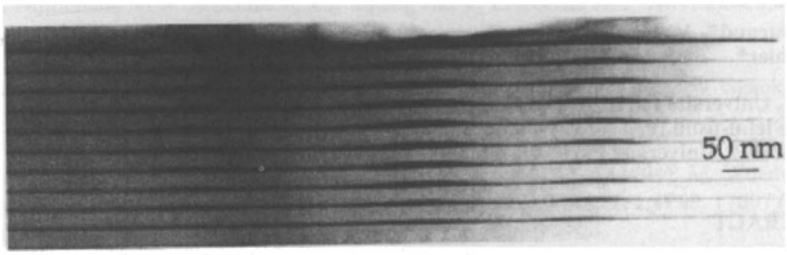

Figure 1. Transmission electronic microscopy image of the Ge/Si multilayer quantum dot sample.

The average quantum dot base width is around 100 nm while the height varies between 4 and 7 nm. For the present growth conditions, the dot density is 2 x 10^9 cm^{-2}. The dot uniformity is estimated as ± 10 %. An atomic force microscopy image of the surface sample is reported in Fig. 2. It appears that the quantum dots have a square based pyramidal shape, oriented along the [100] and [010] directions. The four sidewall facets are mainly formed by {103} and {104} planes.

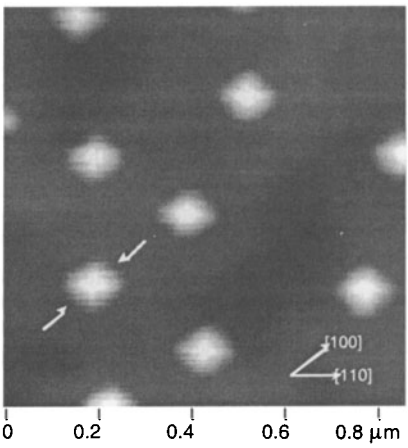

Figure 2. Atomic force microscopy image of the sample surface. The square-based pyramidal quantum dots appear in white contrast.

Photoluminescence

The low-temperature photoluminescence spectrum of the quantum dot sample is reported in Figure 3. Three group of lines can be clearly distinguished. The sharp lines around 1.1 eV are